JOURNAL OF COORDINATION CHEMISTRY, 2016
VOL. 69, NO. 23, 3560–3579
http://dx.doi.org/10.1080/00958972.2016.1241394

Taylor & Francis
Taylor & Francis Group

Platinum(II)-thiosemicarbazone drugs override the cell resistance due to glutathione; assessment of their activity against human adenocarcinoma cells

M. Poyraz[a], S. Demirayak[b], C. N. Banti[c], M. J. Manos[c], N. Kourkoumelis[d] and S. K. Hadjikakou[c]

[a]Faculty of Science and Arts, Chemistry Department, Afyon Kocatepe University, Afyonkarahisar, Turkey; [b]Department of Pharmaceutical Chemistry, Medipol University, Istanbul, Turkey; [c]Inorganic and Analytical Chemistry, Department of Chemistry, University of Ioannina, Ioannina, Greece; [d]Medical Physics Laboratory, Medical School, University of Ioannina, Ioannina, Greece

ABSTRACT

New platinum(II) compounds of the thiosemicarbazone 1-(1H-Benzimidazol-2-yl)ethan-1-one thiosemicarbazone (BzimetTSCH), [Pt(BzimetTSCH)Cl]·2H_2O (**1**) and [Pt(BzimetTSCH)(tpp)]Cl·H_2O·MeCN (**2**) were synthesized. The complexes were characterized by FT-IR spectroscopy and ^{1}H NMR spectroscopy. The crystal structures of **1** and **2** were determined with single-crystal X-ray diffraction analysis. The coordination around platinum is square planar in both complexes. Compounds **1** and **2** were evaluated for their *in vitro* cytotoxic activity against human adenocarcinoma breast (MCF-7) and cervix (HeLa) cells. The apoptotic pathway of cell death was confirmed by cell cycle arrest test. Since deactivation of cisplatin caused by glutathione (GSH) seems to be an important determinant of its cytotoxic effects, the reactions of **1** and **2** with GSH were investigated by UV-absorption spectroscopy. The genotoxicities on normal human fetal lung fibroblast cells (MRC-5) caused by **1** and **2** were evaluated by fluorescence microscopy. The absence of micronucleus in MRC-5 cells confirms the *in vitro* non toxic behavior of the compounds. Moreover, the *in vivo* genotoxicities of **1** and **2** were evaluated by the *Allium cepa* test. Due to negligible genototoxic effect and high antitumor activity which is similar to that of cisplatin, **2** could be a candidate for further study as potential drug since the mitotic index is unchanged.

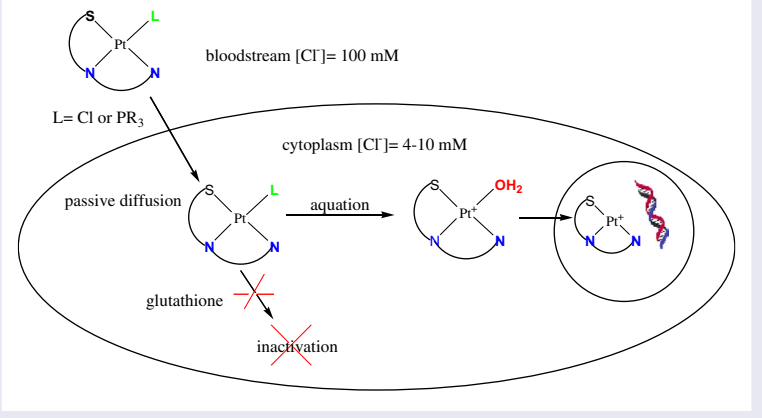

ARTICLE HISTORY
Received 22 July 2016
Accepted 8 September 2016

KEYWORDS
Biological inorganic chemistry; drugs design and development; platinum(II) metallodrugs; cytotoxicity; glutathione; genotoxicity

CONTACT M. Poyraz poyraz@aku.edu.tr; C. N. Banti cbanti@cc.uoi.gr; S. K. Hadjikakou shadjika@uoi.gr
Supplemental data for this article can be accessed at http://dx.doi.org/10.1080/00958972.2016.1241394.

© 2016 Informa UK Limited, trading as Taylor & Francis Group

1. Introduction

Platinum-based drugs such as cisplatin, carboplatin, and oxaliplatin are clinically widely used against different types of tumors [1]. Platinum compounds bind to a variety of cellular targets, especially DNA, causing distortion in DNA backbone and trigger apoptosis to the cancer cells [2]. Platinum complexes exhibit high affinity for sulfur-containing biomolecules, such as amino acids (cysteines and methionines), peptides (glutathione), and proteins (metallothionein) [2, 3]. However, their interaction with intracellular sulfur residues, like glutathione, leads to inactivation of platinum compounds, and thus to cellular resistance against platinum together with toxic side effects [2]. The interactions with the HS-groups of GSH are restricted when the metal complexes have S-bonded ligands [4]. The design of new metallotherapeutics aims for selective metal-based drugs which eliminate cancer cells without toxic effect against normal cells [5]. Especially, platinum(II) and palladium(II) complexes containing N and S donors with anticancer activities exhibit reduced toxicity compared to cisplatin and its analogs [6].

Thiosemicarbazones have shown antibacterial, antifungal, antitumor, and antiviral activities [7]. Thiosemicarbazones where the side chain is attached α to an N-heterocyclic ring, namely α-N-heterocyclic thiosemicarbazones (N-TSCs), are strong metal chelating agents and show antineoplastic activity by interaction toward DNA [8, 9]. Particularly, 3-aminopyridine-2-carboxaldehyde thiosemicarbazone (Triapine, Vion Pharmaceuticals, New Haven, CT) has been selected for Phases I and II clinical trials for antitumor therapy [9]. Thiosemicarbazone complexes of platinum(II) have proven to be chemotherapeutic agents due to synergistic effect of the pharmacological properties of both ligands and metal [10–12].

Only three structures of metal complexes with 1-(1H-benzimidazol-2-yl)ethan-1-one thiosemicarbazone (BzimetTSCH) [13] are reported. These include the structures of $[BzimetTSC]_2Ni$ [14], $([Zn(NO_3)(H_2O)(BzimetTSC)]NO_3)$ [15], and [Co(BzimetTSC) (BzimetTSCH)] [16]. The antimicrobial activity of $([Zn(NO_3)(H_2O)(BzimetTSC)]NO_3)$ and [Co(BzimetTSC)(BzimetTSCH)] were evaluated against Gram-positive, Gram-negative bacteria, and the fungi *Candida albicans*, showing moderate activity [15, 16].

In the course of our studies on the design and development of new metallotherapeutics [17–23], we have prepared two new platinum complexes of BzimetTSCH (scheme 1), $[Pt(BzimetTSCH)Cl]\cdot 2H_2O$ (**1**) and $[Pt(BzimetTSCH)(tpp)]Cl\cdot H_2O\cdot MeCN$ (**2**) (tpp = triphenylphosphine). Compounds **1** and **2** were characterized by IR, ^1H NMR and single-crystal X-ray diffraction (XRD) analysis. BzimetTSCH was chosen in order to form stable complexes with Pt(II) which will be able to override the interaction with glutathione and reduce cellular resistance. To evaluate the deactivation of **1** and **2** caused by glutathione, the reactions of **1** and **2** with glutathione (GSH) were investigated by UV-absorption spectroscopy. Compounds **1** and **2** were also used to investigate the influence of the lipophilicity on cancer cell viability, since increasing lipophilicity is expected to improve the permeability of the massive compounds to cell membranes and the activity of metal–phosphine complexes toward cancer cells [24]. Compounds **1** and **2** and BzimetTSCH were tested for their *in vitro* antiproliferative activity against the human adenocarcinoma cells, MCF-7 (breast) and HeLa (cervix), and the non cancerous cells, MRC-5 (fetal lung fibroblast). The genotoxicities on normal human fetal lung fibroblast cells (MRC-5) caused by **1** and **2** were evaluated by fluorescence microscopy, *in vitro*. The *in vivo* genotoxicity of **1** and **2** were evaluated by the *Allium cepa* test.

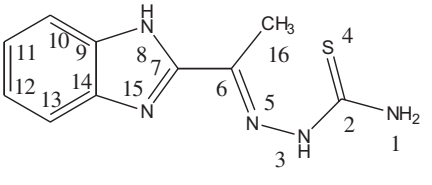

Scheme 1. The molecular formula of 1-(1H-Benzimidazol-2-yl)ethan-1-one thiosemicarbazone.

2. Results and discussion

2.1. General aspects

Complex **1** was synthesized from the reaction between BzimetTSCH and $PtCl_2$ in ethanol/water solution under reflux, while **2** was derived by refluxing acetonitrile/ethanol solution of BzimetTSCH, tpp, and $PtCl_2$. Red needle crystals of **1** have been grown from slow evaporation of acetonitrile solution after recrystallization, while reddish-orange prismatic crystals of **2** were grown from the filtrate of the mother solution after reflux. The formulas of the compounds were initially detected with spectroscopic methods and their structures were determined by single-crystal X-ray diffraction analysis. The crystals of **1** and **2** are air stable when they are stored in the dark at room temperature.

2.2. Solid-state studies

2.2.1. Vibrational spectroscopy

The asymmetric and symmetric stretching of $\nu(NH_2)$ and ν(NH) bonds, respectively, at 3368, 3181, 3071 cm^{-1} in the IR spectrum of free ligand BzimetTSCH undergo negligible shifts in **1** and **2**, suggesting the non-coordination of the terminal NH_2 and N–H of imidazole (figures S1–S3) [25]. The band at 3426 cm^{-1} assigned to ν(O–H) of free ligand remained in the spectra of the complexes due to the water molecules co-crystallized.

The bands at 1624 and 842 cm^{-1} in **1** and at 1615 and 839 cm^{-1} in **2** are attributed to ν(C=N) and ν(C=S), respectively. Coordination of the azomethine nitrogen to the metal ion is supported by shift of the vibrational band of ν(C=N) to higher wavenumbers in **1** and to lower wavenumbers in **2** [16]. Coordination of sulfur causes, in the spectra of both complexes, shift of the ν(C=S) band at 842(**1**) and 839(**2**) cm^{-1} to lower frequency [26]. The bands at 515 and 501 cm^{-1} are attributed to ν(C–P) in **2** (figure S4).

2.2.2. Crystal and molecular structure of [Pt(BzimetTSCH)Cl]·$2H_2O$ (1) and [Pt(BzimetTSCH(tpp)]Cl·H_2O·MeCN (2)

ORTEP diagrams of **1** and **2** along with their selected bond distances and angles are shown in figures 1 and 2. In the case of **1**, one Cl^- and one BzimetTSCH are coordinated to Pt(II) forming a square planar geometry. The BzimetTSCH is coordinated tridentate through S1,N3,N1. Two water molecules are co-crystallized. One phosphorus from tpp, two nitrogens, and one sulfur (N3,N2,S1) from BzimetTSCH form a square planar geometry around platinum(II) in **2**. The net charge in **2** is balanced by a chloride counter anion. The bond distances around platinum in **1** are: Pt1–S1 = 2.2505(12), Pt1–N1 = 2.048(3), Pt1–N3 = 1.974(4), and Pt1–Cl1 = 2.3140(11) Å, while the corresponding bond distances in **2** are Pt1–S1 = 2.249(2), Pt1–N3 = 2.057(6), Pt1–N2 = 2.092(6), and Pt1–P1 = 2.257(2) Å. The C10–S1 bond distance varied from 1.697(4) Å in free ligand, to 1.748(4) (**1**) and 1.763(8) Å in **2**, respectively [16]. The N4–C10 bond length is 1.351 Å in free BzimetTSCH, while for **1** it is 1.328(5) Å and 1.318(9) Å for **2**. This shortening is a consequence of the coordination of the ligand to platinum.

The angles around platinum(II) ion deviate from the ideal value of 90° due to electrostatic repulsions among valance shell electron pairs (VSEPR theory). The angles are Cl1–Pt1–S1 = 95.48(4), Cl1–Pt1–N1 = 98.93(9), Cl1–Pt1–N3 = 178.76(11), S1–Pt1–N1 = 165.58(8), S1–Pt1–N3 = 84.92(10), and N1–Pt1–N3 = 80.67(13)° in **1**, while in **2** they are P1–Pt1–S1 = 94.25(7), P1-Pt1-N2 = 103.46(18), P1–Pt1–N3 = 177.17(16), S1–Pt1–N2 = 162.29(19), S1–Pt1–N3 = 83.51(17), and N2–Pt1–N3 = 78.8(2)°.

2.3. Solution studies

Since ligand displacement and changes to the structure of the platinum drugs cisplatin, carboplatin, and oxaliplatin occurred upon their dilution in DMSO [27], the stability of **1** and **2** in DMSO solutions was tested by UV–vis (figure S5) spectra and ^{1}H NMR (figures S6 and S7) measurements for a period of 48 h in DMSO-d_6 solutions. The 48 h was chosen since this is the incubation period of the cells with

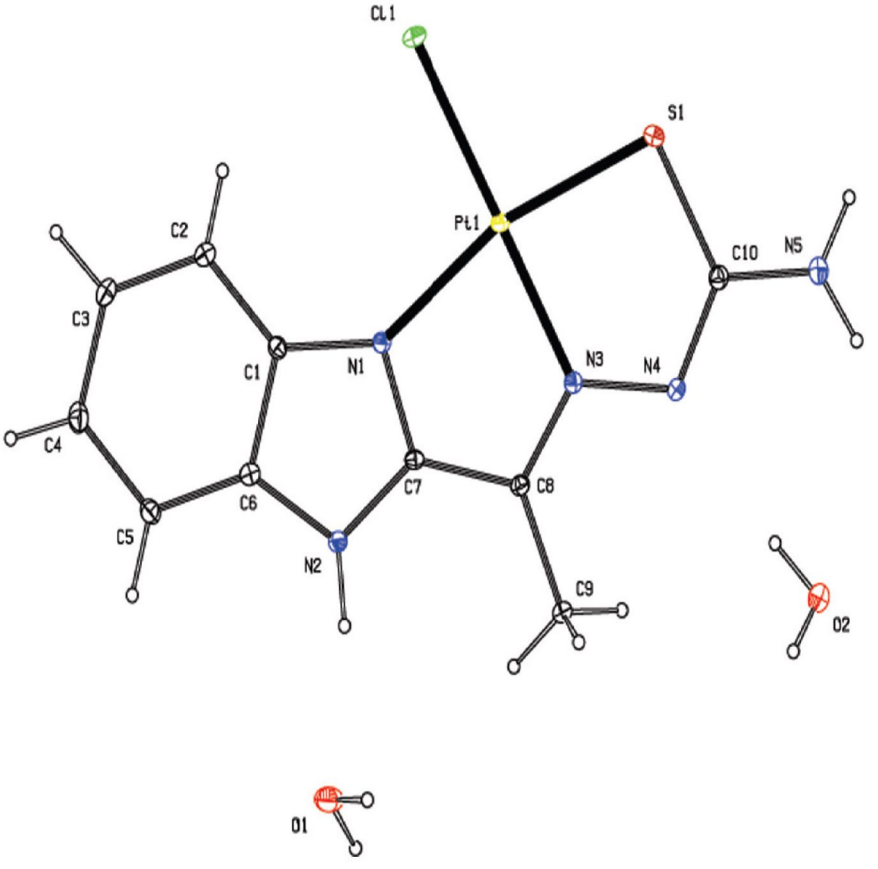

Figure 1. ORTEP diagram together with the numbering of **1**. Selected bond lengths (Å) and angles [°]: Pt1–Cl1 = 2.3140(11), Pt1–S1 = 2.2505(12), Pt1–N1 = 2.048(3), Pt1–N3 = 1.974(4), N3–N4 = 1.375(5), Cl1–Pt1–S1 = 95.48(4), Cl1–Pt1–N1 = 98.93(9), Cl1–Pt1–N3 = 178.76(11), S1–Pt1–N1 = 165.58(8), S1–Pt1–N3 = 84.92(10), N1–Pt1–N3 = 80.67(13).

metal drugs during the biological experiments. No changes were observed between the initial UV or ^{1}H NMR spectra and the corresponding spectra after 48 h confirming retention of the structures in solution.

2.3.1. ^{1}H NMR studies

The ^{1}H NMR spectrum of the BzimetTSCH (figure S8) is dominated by the signals at 12.69, 10.66, and 2.40 ppm which are attributed to H(^{3}N, s), H(^{8}N,s), and H($^{16}CH_3$–, s) (scheme 1). The absence of H(^{3}N) resonance signal in the ^{1}H NMR spectra of **1** and **2**, which is observed at 12.70 ppm in the spectrum of BzimetTSCH (figure S8), suggests coordination of the drug to platinum through N and S donors. The broad signals at 8.41 ppm in **1** and 8.16 ppm in **2** are assigned to H(^{8}N) which is shifted due to coordination. The signal at 2.25 ppm in **1** and at 2.55 ppm in **2** correspond to the H(^{16}C) of the CH_3– group. The assignment of the ^{1}H NMR spectra of both **1** and **2** is based on their crystal structure and indicates the coordination of the ligands to platinum and retention of the structures in DMSO solution.

2.3.2. ^{31}P NMR studies

The ^{31}P NMR spectrum of **2** confirms the retention in DMSO-d_6 solutions. The signal at –6.849 ppm of tpp is shifted at 7.240 ppm in **2** upon coordination (figure S9).

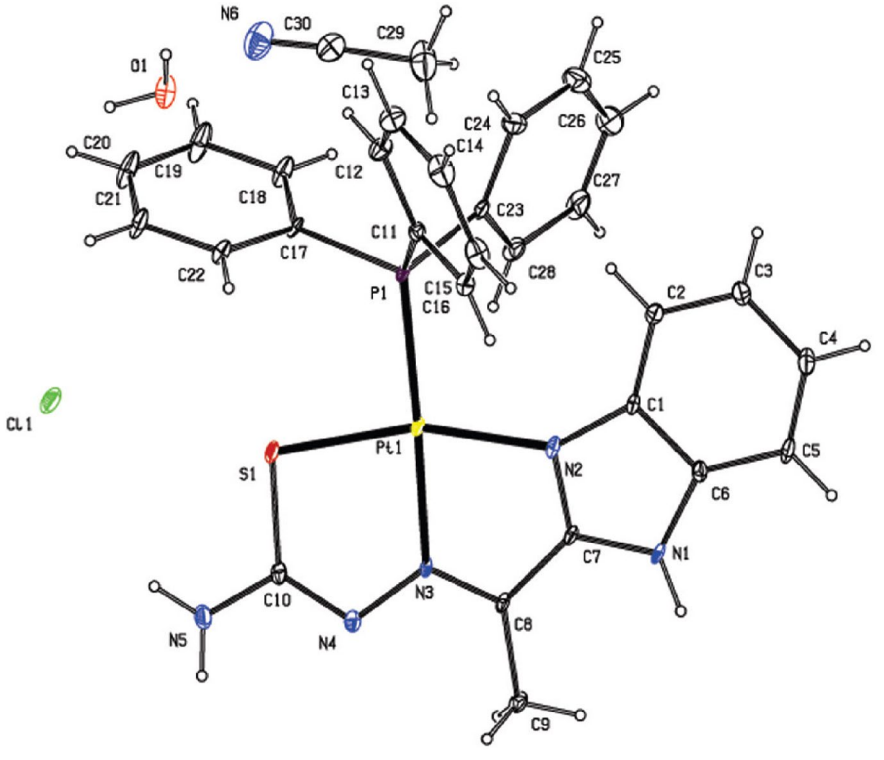

Figure 2. ORTEP diagram together with the numbering scheme of **2**. Selected bond lengths (Å) and angles [°]: Pt1–S1–2.249(2), Pt1–P1 = 2.257(2), Pt1–N2 = 2.092(6), Pt1–N3 = 2.057(6), P1–Pt1–S1 = 94.25(7), P1–Pt1–N2 = 103.46(18), P1–Pt1–N3 = 177.17(16), S1-Pt1-N2 = 162.29(19), S1–Pt1–N3 = 83.51(17), N2–Pt1–N3 = 78.8(2).

2.4. Biological tests

2.4.1. Antiproliferative activity

Complexes **1** and **2** and BzimetTSCH were tested for their *in vitro* antiproliferative activity against two human adenocarcinoma cell lines, MCF-7 (human breast adenocarinoma cell line), and HeLa (human cervix adenocarcinoma cell line), by the SRB assay after 48 h of incubation. The IC_{50} values are summarized in table 1. The lower IC_{50} value is exhibited by **2** (8.8 ± 0.4 (**2**) and 13.1 ± 0.4 (**1**) μM, respectively). Complex **2** exhibits five times higher activity than **1**, against MCF-7 cells. The same trend applies against HeLa cells (1.5 times higher activity). Moreover, **2** shows better antiproliferative activity than cisplatin against both cell lines (the IC_{50} values of cisplatin are 5.5 and 3.9 μM, respectively). Compounds which contain tpp are generally more active against MCF-7 or HeLa (table 1) [28, 29]. This might be attributed to the higher lipophilicity introduced by tpp and through this to better membrane permeability of the platinum complexes.

The toxicities of BzimetTSCH, **1** and **2** are evaluated against normal human fetal lung fibroblast cells (MRC-5 cells) (table 1). The IC_{50} values of **1** and **2** are 16 ± 1 (**1**) and 4.8 ± 0.4 (**2**) μM, respectively. The therapeutic potency or selectivity of a metallotherapeutic agent could be surveyed by the therapeutic potency index (TPI). TPI is defined as the IC_{50} value against normal cell line divided by IC_{50} value against cancer cell line of the same or similar tissue. Therefore, the higher the TPI value the better potency of the metallotherapeutic agent [18]. For MCF-7 cells, the TPI for **1** and **2** are 0.9 and 1.3, respectively, while against HeLa are 1.2 and 0.5. The corresponding TPI values for the cisplatin are 0.2 and 0.3 against

Table 1. Metal complexes against two adenocarcinoma cell lines MCF-7 (breast), HeLa (cervix), and normal human fetal lung fibroblast cells (MRC-5 cells).

Complexes	IC_{50} (μM)			Ref.
	MCF-7	HeLa	MRC-5	
1	17.1 ± 0.7	13.1 ± 0.4	15.7 ± 1.2	*
2	3.6 ± 0.4	8.8 ± 0.4	4.8 ± 0.4	*
BzimetTSCH	>30	>30	>30	
$PtCl_2L1$		37		[10]
$PtCl_2L2$		37		[10]
$PtCl_2L3$		105		[10]
$PtCl_2L4$		1.7		[10]
$PtCl_2L5$		46		[10]
[PtL6] DMSO	>100			[8]
[PtL7] DMSO	44 ± 2			[8]
$[Pt(H_3L8)]_2$	>100			[28]
$Pt(L9)(PPh_3)$	1.49 ± 0.04			[29]
Cisplatin	5.5 ± 0.4	3.9 ± 0.1	1.1 ± 0.2	[21, 22]

This work; L1 = Thiophene-2-carboxaldehyde-N(4)phenyl thiosemicarbazone; L2 = 5-Chlorothiophene-2-carboxaldehyde-N(4)phenyl thiosemicarbazone; L3 = 5-Phenylthiophene-2-carboxaldeyde-N(4)phenyl; L4 = 5-Nitrothiophene-2-carboxaldehyde-N(4) phenyl thiosemicarbazone; L5 = Thiophene-2-carboxaldehyde-N(4)nitrophenyl thiosemicarbazone; L6 = 2,6-diacetylpyridine bis(^{4}N-o-tolylthiosemicarbazone), L7 = 2,6-diacetylpyridine bis(^{4}N-p-tolylthiosemicarbazone; L8 = [3,5-diacetyl-1,2,4-triazol bis(4-cyclohexylthiosemicarbazone); L9 = Thiosemicarbazone- derived from indole-7-carbaldehyde.

Table 2. Physico-chemical properties for Pt complexes with thiosemicarbazones.

Complexes	Dipole (D)[a]	E HOMO (eV)[a]	E LUMO (eV)[a]	LogP	HBD	HBA	Volume	Polar Surface Area	Molecular Surface Area	Molecular polarizability
1	8.92	−8.24	−2.01	1.96	2	6	293.13	56.56	362.85	36.31
2	4.88	−6.52	−0.69	5.93	2	6	486.37	56.56	779.72	68.42
[PtL7] DMSO	7.84	−8.05	−2.23	6.65	2	9	474.89	57.84	736.99	66.14
$[Pt(H_3L8)]_2$	3.32	−8.22	−1.03	9.86	3	11	706.67	90.96	1142.76	94.82
$Pt(L9)(PPh_3)$	6.32	−7.78	−1.09	5.72	1	5	478.15	44.53	759.36	66.89

[a]PM6 L7 = 2,6-diacetylpyridine bis(^{4}N-p-tolylthiosemicarbazone; L8 = [3,5-diacetyl-1,2,4-triazol bis(4-cyclohexylthiosemicarbazone); L9 = Thiosemicarbazone- derived from indole-7-carbaldehyde.

MCF-7 and HeLa cells, respectively (table 1). BzimetTSCH has no effect to proliferation of cancerous or non-cancerous cells. In conclusion, **2** exhibits stronger cytotoxic activity against adenocarcinoma cells, selectivity against cancerous cells, while it exerts comparable activity with cisplatin.

2.4.2. Computational study

Platinum compounds of tpp exhibit better cytotoxic activity than those without (table 1), which might be attributed to the higher lipophilicity introduced by tpp (see above). Theoretical calculations were performed to rationalize the influence of steric and electronic factors involved in the activity of the compounds. Thus, the dipole moment and frontier orbital energies were calculated by single point energy calculations at the semi-empirical PM6 level (table 2) [30]. The other properties in table 2 were calculated using ChemAxon software available at (http://www.chemicalize.org). All properties were assessed for **1** and **2** as well as known crystal structures which are included in table 1. The results confirm our assumption about the influence of the lipophilicity on the compound's activities since compounds of higher LogP (higher lipophilicity) exhibit better cytotoxicity (tables 1 and 2).

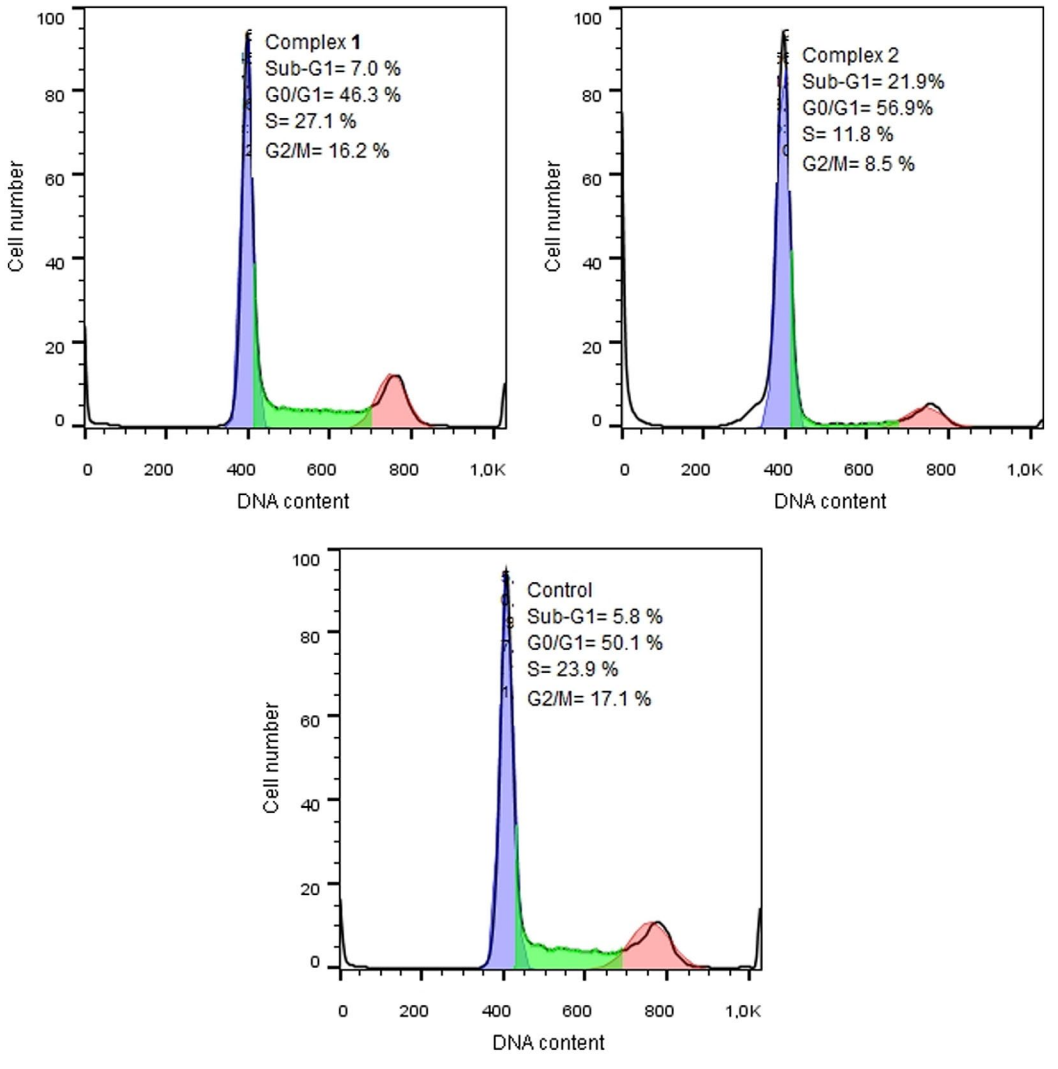

Figure 3. Effects of **1** and **2** on cell cycle against MCF-7 cells. The relative number of cells within each cell cycle was determined by flow cytometry. Number of cells in sub-G_1, G_0/G_1, S, and G_2/M phase are indicated.

2.4.3. Cell cycle

In order to rationalize the mechanism of action of **1** and **2** flow cytometry was employed. Since a characteristic of apoptosis is the internucleosomal DNA fragmentation, the apoptotic cells can be identified as a consequence on DNA content frequency histograms with fractional (sub-G1 peak) DNA content [31, 32].

The possible effect of **1** and **2** on the progression of cell cycle was performed to quantify the percentage of MCF-7 cells which undergo apoptosis giving a sub-G_1 peak. Exponentially growing MCF-7 cells were treated with **1** and **2** in their IC_{50} values for 48 h, stained with propidium iodide, and the amount of DNA was analyzed by flow cytometry. Figure 3 illustrates the pronounced effects on the cell cycle caused from **1** and **2**. The control cells (not treated cells), are spread in 5.8% sub-G_1 phase, 50.1% in G_0/G_1, 23.9% in S, and 17.1% in G_2/M phase. After incubation of the MCF-7 cells with **1** and **2**, an increase in the number of apoptotic cells in sub-G_1 phase (7.0% (**1**) and 21.9% (**2**)) was observed compared to the control group (5.8%). The percentage of cells in the S phase, however, was increased to 27.1% with **1**. The percentage of the non-treated cells in the S phase is 23.9%. Thus, **1** suppresses cell proliferation

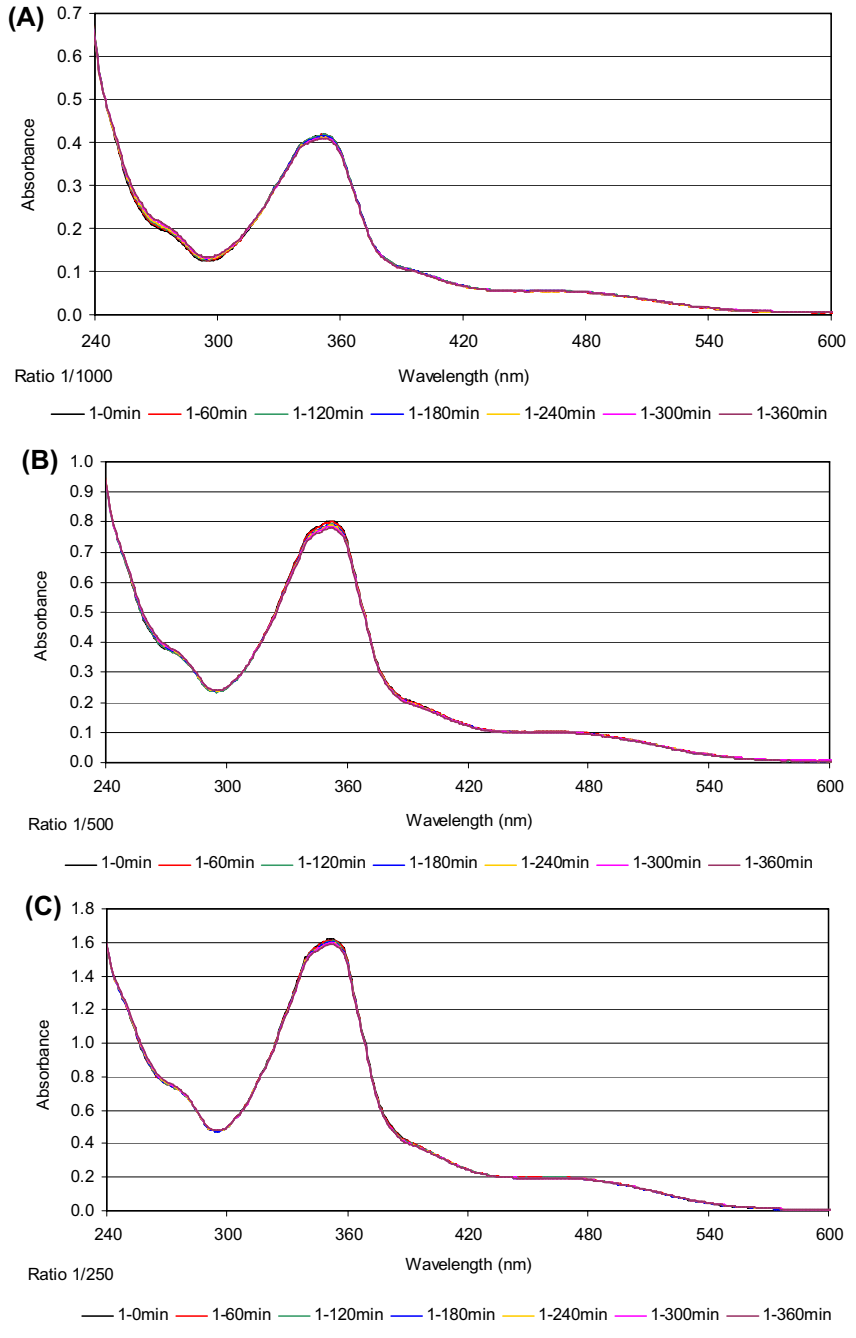

Figure 4. Initial UV spectra of the solutions (final volume of 2.0 mL) containing different concentrations of **1**, 16.5 (A), 33 (B), and 66 (C) µM in 100 mM Tris HCl, pH 7.4 with a high excess of GSH (16.5 mM) at 37 °C and after 1, 2, 3, 4, 5, and 6 h.

by inhibiting DNA synthesis and inducing S phase cell cycle arrest [33]. The percentage of cells in the G_0/G_1 phase when they are treated with **2** is increased to 56.9%, while the non-treated cells (control) show 50.1% cells in the G_0/G_1 phase (figure 3). MCF-7 cells were blocked by **2** during the G_0/G_1 transition and the number of apoptotic cells increased significantly after 48 h of incubation. Cisplatin analogs

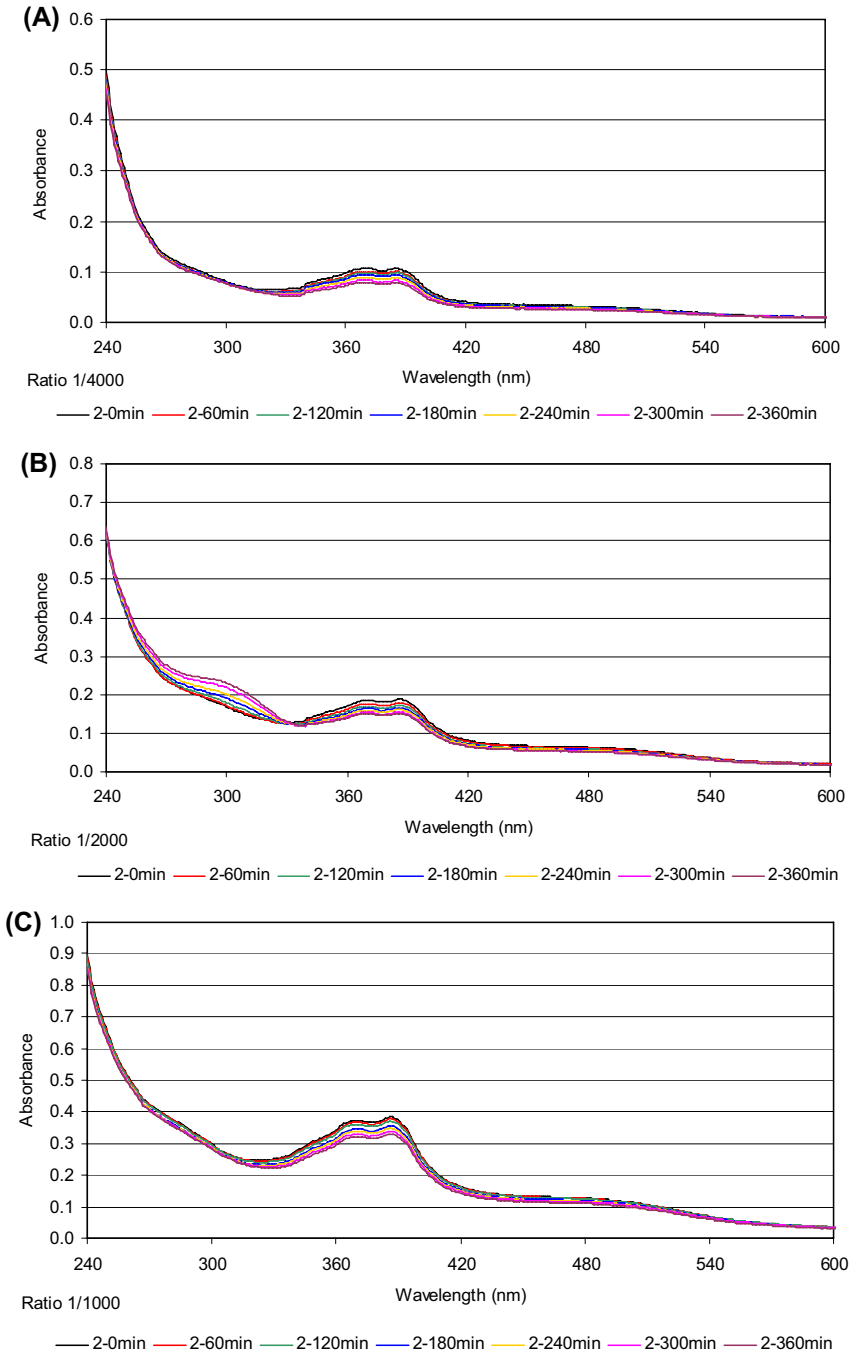

Figure 5. Initial UV spectra of the solutions (final volume of 2.0 mL) containing different concentrations of **2**, 4.2 (A), 8.3 (B), and 16.5 (C) μM in 100 mM Tris HCl, pH 7.4 with a high excess of GSH (16.5 mM) at 37 °C and after 1, 2, 3, 4, 5, and 6 h.

(*cis*-[$PtCl_2(CH_3SCH_2CH_2SCH_3)$], *cis*-[$PtCl_2(DMSO)_2$]), at IC_{50} concentrations, increased the number of MCF7 cells in G_0/G_1 phase of cell cycle [34].

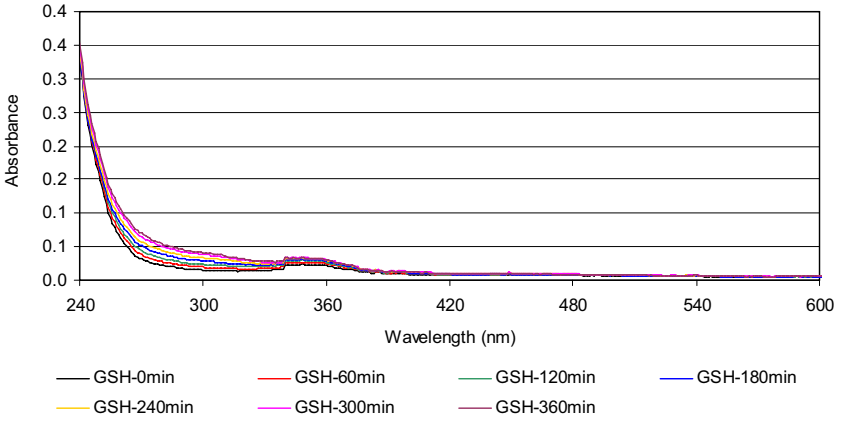

Figure 6. UV absorption spectra of GSH *vs*. time.

2.4.4. Reaction of **1** *and* **2** *with GSH as monitored by UV absorption*

The deactivation of cisplatin, caused by glutathione, is an important determinant of cytotoxic effects. Thus, the reactions of **1** and **2** with glutathione (GSH) were investigated and the results are compared with the binding affinity of GSH to cisplatin [4]. The presence of sulfur from thiosemicarbazone ligand in the coordination sphere is expected to eliminate the cell resistance against the metallotherapeutic compounds through GSH. The initial UV spectra of the solutions contain different concentrations of **1** (16.5 (A), 33 (B) and 66 (C) μM) or **2** (4.2 (A), 8.3 (B) and 16.5 (C) μM) in 100 mM Tris-HCl, pH 7.4 with a high excess of GSH (16.5 mM) at 37 °C and after 1, 2, 3, 4, 5, and 6 h are shown in figures 4 and 5. Increasing of absorption intensity in time is due to (i) the reaction of metal complex with GSH (formation of metal-sulfur bonds) and (ii) to the oxidation of GSH (formation of the disulfide GSSG). The diagram of absorption *versus* time for GSH alone is shown in figure 6. However, as the rate of disulfide formation is slow, the concentration of GSH was assumed not to change much, over time during the GSH–complex reaction. Because the GSH concentration is 250 or 1000 fold higher than that of **1** or **2**, respectively, the reaction does not deplete GSH. The absorbance associated with GSH–complex formation is obtained by abstracting the absorbance due to disulfide from the observed absorbance (figures 7 and 8). The difference shows the change in absorption for reaction of a complex with GSH (because the rate of disulfide formation is not important in the presence of metal complexes). Although **1** or **2** and Pt-GSH products absorb at 260 nm, the extinction coefficients of the products are much greater than those of **1** or **2** [35, 36]. Thus, the absorbance at 260 nm is mainly due to formation of Pt-GSH products. Figures 7 and 8 show no increase in absorption, indicating no complex–GSH formation. Thus, **1** and **2** undergo no deactivation from GSH in contrast to cisplatin [4, 36].

2.4.5. Evaluation of genotoxicity by micronucleus assay

The presence of micronuclei (MN) is a biomarker of mutagenic, genotoxic, or teratogenic agent influence [37]. The MN can be formed during the transition metaphase–anaphase of the mitosis, upon influence of an exogenous factor (such as chemical agents). The MN appears as small membrane bound DNA fragments in the cytoplasm of interphase cells [38]. The MN is unable to be incorporated to daughter cells [37]. The micronucleus assay has been used in monitoring genetic damage in different tissue and cell types [39]. Human cell lines in culture are sensitive tools for toxicity screening and they are capable of reducing the use of animals in toxicological testing [40].

In order to ascertain the genotoxicity of **1** and **2** against MRC-5 normal cells (see above), the possible inductions of micronucleus frequencies was checked. The micronucleus frequencies in the MRC-5 cell culture without treatment is 0.8%, which becomes 0.56% after treatment with DMSO. No micronuclei (0.8%) were detected when **1** was used. Although, a slight increase in the micronucleus frequencies is

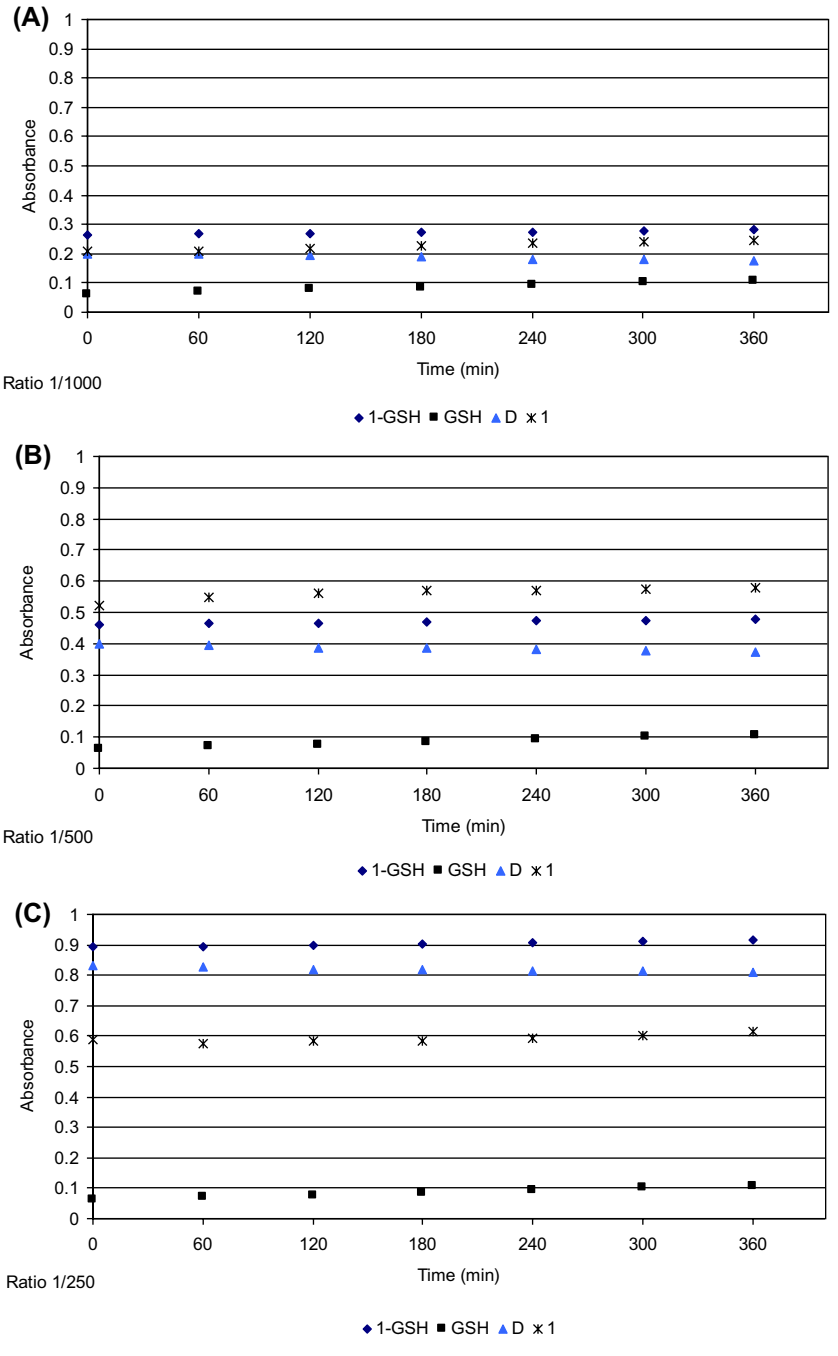

Figure 7. Absorbance at 260 nm for different concentrations of **1**, 16.5 (A), 33 (B), and 66 (C) µM incubated with GSH (16.5 mM) in 100 mM Tris HCl, pH 7.4, buffer containing 5 mM NaCl at 37 °C *vs.* time (0–6 h) (♦), GSH (■), the complex (✳), and the points derived from the subtraction among them (D curve) (▲).

observed when the cells were treated with **2** (1.0%) (figure 9). Therefore, **1** causes no genetic damage to normal cells, indicating no mutagenic, genotoxic, or teratogenic. Complex **2** on the other hand seems to be slightly more genotoxic than **1**.

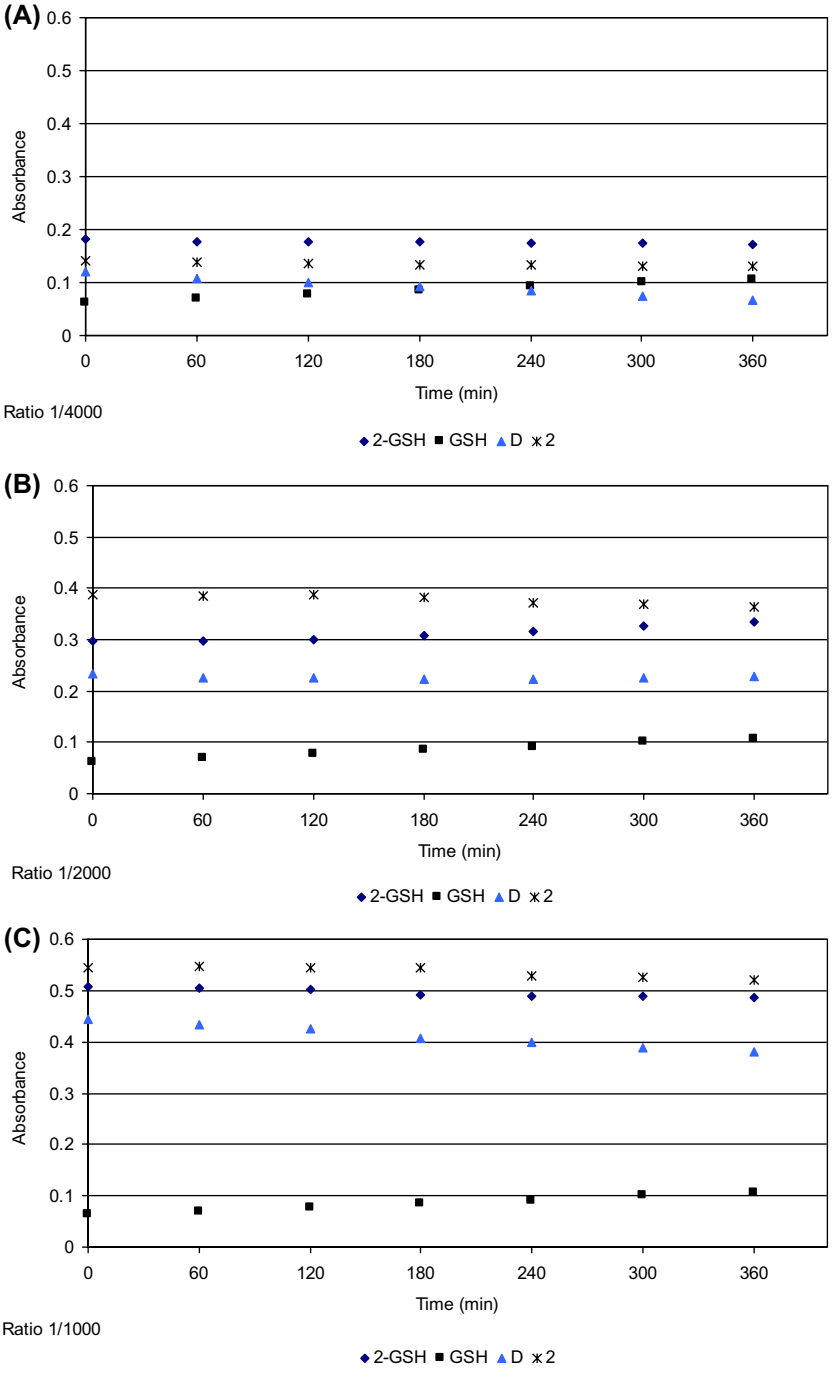

Figure 8. Absorbance at 260 nm for different concentrations of **2**, 4.2 (A), 8.3 (B), and 16.5 (C) μM incubated with GSH (16.52 mM) in 100 mM Tris HCl, pH 7.4, buffer containing 5 mM NaCl at 37 °C *vs.* time (0–6 h) (◆), GSH (■), the complex (✳), and the points derived from the subtraction among them (D curve) (▲).

2.4.6. In vivo *genotoxicity test*

The development of new drugs requires assessment of their potential toxicity. The *Allium cepa* test is an experimental model which has been employed to evaluate the *in vivo* potential genotoxicity of **1**

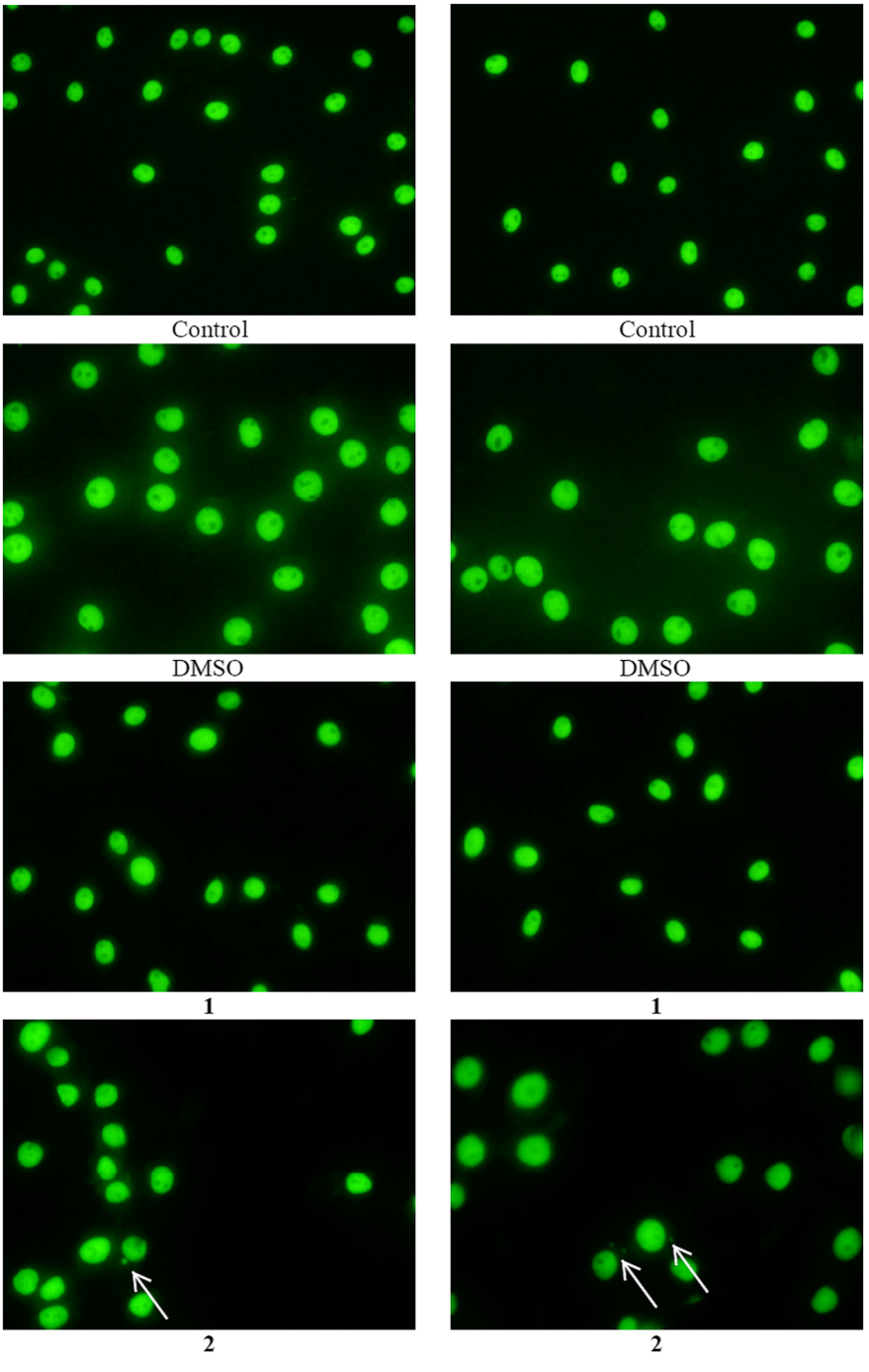

Figure 9. Micronucleus formed in MRC-5 cells treated with IC_{50} values of **1** and **2** for a period of 48 h; arrow indicates micronucleus in MRC-5 cells.

and **2**, since it is crucial in the development of new metallotherapeutics [19, 22, 41]. *Allium cepa* show high correlation with mammal test systems [41].

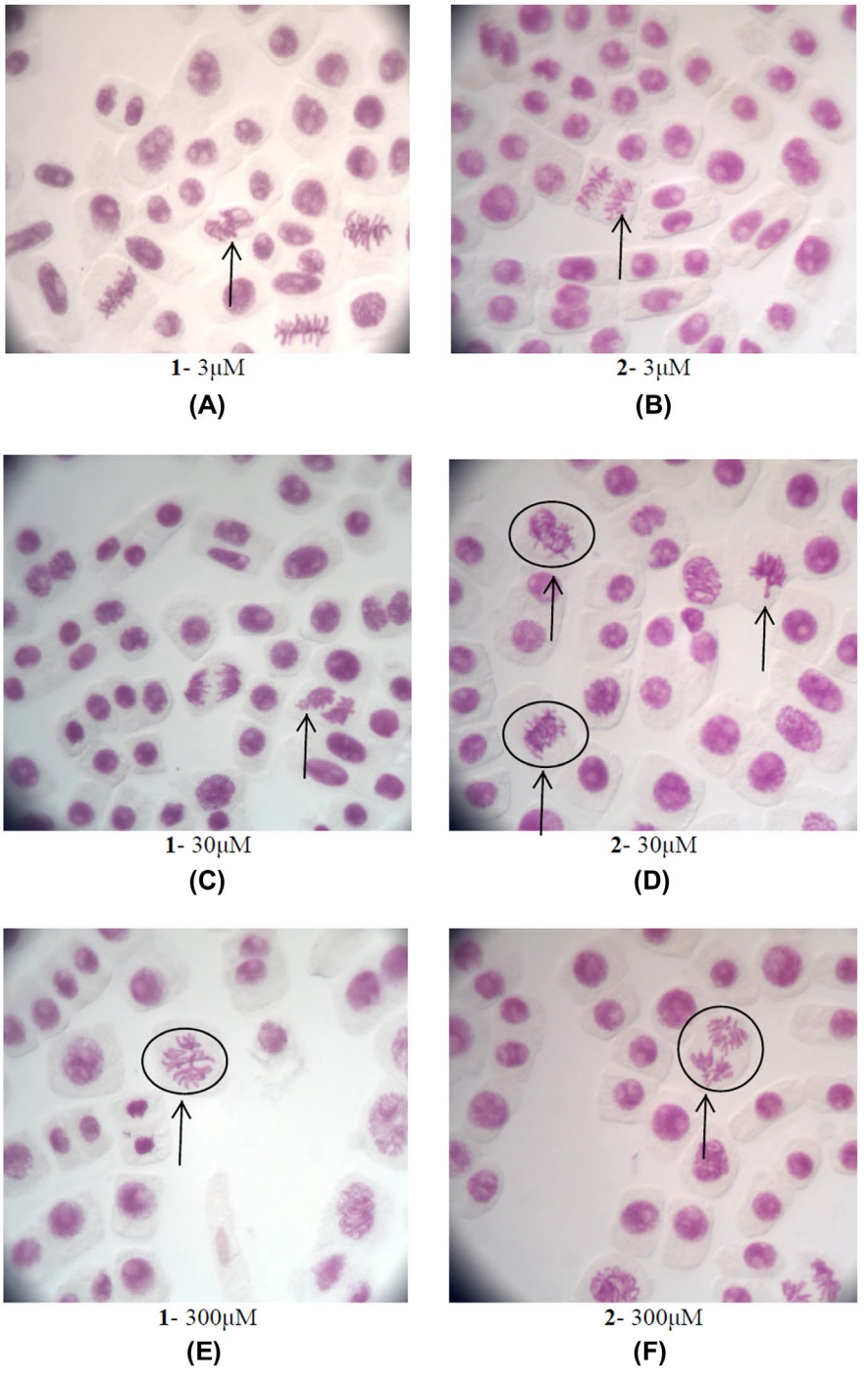

Figure 10. *Allium cepa* meristematic cells exposed to **1** and **2**. (A) *Allium cepa* meristematic cells exposed with 3 μM of **1**. Metaphase with chromosome adherence (B) *Allium cepa* meristematic cells exposed with 3 μM of **2**. Chromosome losses and bridges at anaphase (C) *Allium cepa* meristematic cells exposed with 30 μM of **1**. Anaphase with chromosome adherence (D) *Allium cepa* meristematic cells exposed with 30 μM of **2**. Chromosome aberration, anaphase with chromosome bridge, and loss observed. Chromosome losses at telophase (E) *Allium cepa* meristematic cells exposed with 300 μM of **1**. Chromosome aberration, anaphase with chromosome bridge and loss observed. (F) *Allium cepa* meristematic cells exposed with 300 μM of **2**. Chromosome aberration, anaphase with chromosome bridge and loss observed.

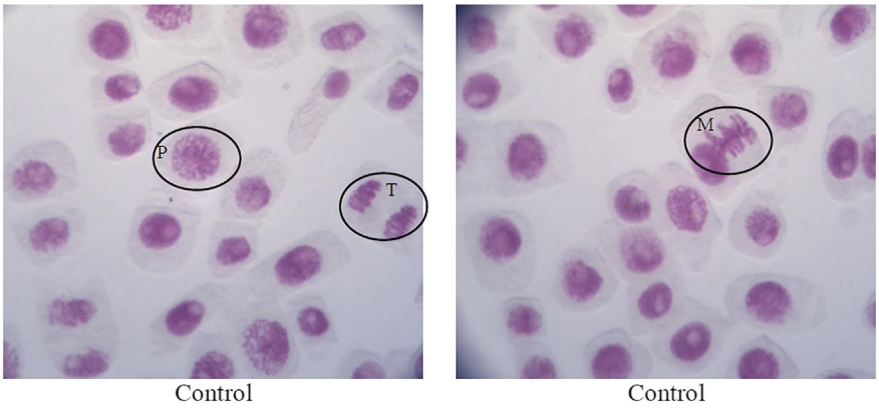

Figure 11. Normal prophase (P), metaphase (M), and telophase (D) in *Allium cepa* meristematic cells in negative control.

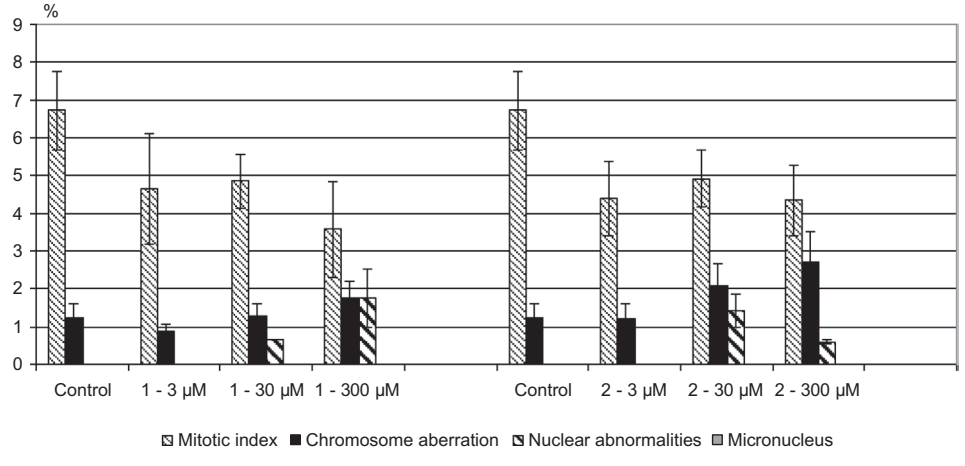

Figure 12. The mitotic index % (MI), the chromosomal aberrations (%), the nuclear abnormalities (%), and the micronucleus (%) observed when *Allium cepa* was incubated with **1** and **2**.

The mitotic index % (MI) is defined as the ratio between the cells in a population undergoing mitosis to the cells not undergoing mitosis [19, 22, 41].

The decrease in the mitotic index (MI) of *Allium cepa* can be considered as a reliable method to determine the presence of a cytotoxic agent. DNA damages are assessed such as chromosome aberrations (CA), nuclear abnormalities (NA), and presence of micronucleus (MN). CA is characterized by changes in either chromosomal structure or in the total number of chromosomes [19, 22, 41]. The CA includes chromosome bridges and breaks and are indicators of a clastogenic action, whereas chromosome losses, delays, and adherence result from aneugenic effects. NA are characterized by morphological alterations in the interphasic nuclei, as a result of exposure in the tested agent. These alterations are observed as lobulated nuclei, nuclei carrying nuclear buds, polynuclear cells, and mini cells. MN are considered as the most effective and simplest endpoint to analyze the mutagenic effect.

The decreasing of the mitotic index observed when *Allium cepa* is incubated with **1** or **2** at 3, 30, and 300 µM for 48 h was associated with appearance of chromosome aberrations (%), the nuclear abnormalities (%), and the micronucleus (%) (figure 10). The range of the concentrations studied contains the IC_{50} values of **1** and **2** against the cells (table 1). Figure 11 shows the normal prophase, metaphase, and telophase in *Allium cepa* meristematic cells in the negative control.

Analysis of the mitotic index (MI) reveals a decreasing of cell division index at 300 μM for **1** and **2** (MI is 3.6% (**1**), 4.3% (**1**) toward 6.7% of the control) (figure 12). The MI of the cell division of *Allium cepa* is affected when they are treated with **1** or **2** with 300 μM, indicating they are mutagenic or genotoxic.

The effect in mitotic index caused by **1** or **2** is associated with alteration in the chromosome aberrations (CA) and the presence of nuclear abnormalities (NA). Chromosome aberrations of *Allium cepa* in mesophase, metaphase, anaphase, and telophase are shown in figure 12. An increase in the chromosome aberrations was observed by treatment of *Allium cepa* with **1** and **2** at the highest concentration of 300 μM (CA = 1.8 (**1**) and 2.7 (**2**) %, respectively) toward the negative control (CA = 1.3%). The most common chromosome aberrations observed are sticky, bridges, and loss chromosomes (figure 9). Moreover, an increase NA with **1** and **2** at the highest concentration of 300 μM (NA = 1.8 (**1**) and 0.6 (**2**) %, respectively) is observed toward the negative control (NA = 0%). No MN were observed in accordance with the findings of *in vitro* genotoxicity studies (see genotoxicity by micronucleus assay).

3. Conclusion

[Pt(BzimetTSCH)Cl]·2H_2O (**1**) and [Pt(BzimetTSCH)(tpp)]Cl·H_2O·MeCN (**2**) with square planar geometry were developed to investigate (a) the influence of the lipophilicity since the tpp is expected to improve the permeability of the massive compounds to cell membranes and activity of metal–phosphine complexes toward cancer cells and (b) the higher stability of Pt-thiosemicarbazone than the corresponding Pt-glutathione which might be formed in cytoplasm, a factor causing cell resistance to platinum containing anticancer drugs. Compounds **1** and **2** were tested for their antiproliferative activity against human adenocarcinoma breast (MCF-7) and cervix (HeLa) cells. Complex **2** which contains tpp exhibits better cytotoxic activity against MCF-7 cells (five times higher activity against MCF-7) than **1** without tpp. The same trend also appears against HeLa cells. Mixed ligand Pt(II) complexes of thiosemicarbazones and tpp are more active against MCF-7 or HeLa (table 1). The increase in the number of apoptotic cells in sub-G_1 phase (7.0% (**1**) and 21.9% (**2**)) toward the control group (5.8%) suggest apoptotic mechanism of action of **1** and **2**, with **2** showing stronger activity. The [(1R,2R)-N1–2-amyl-1,2-cyclohexanediamine-N,N′](malonato-O,O′)platinum(II) inducing apoptosis and arresting cells in the G_2 phase against HepG2 cells was also shown [42]. The higher cytotoxicity and apoptotic activity of **2** are attributed to the higher lipophilicity due to the presence of tpp, which leads to better membrane permeability. Computations further support the influence of lipophilicity since compounds with higher logP, generally, exhibit better activity. The reaction of **1** and **2** with GSH show that **1** and **2** undergo no interaction with GSH in contrast to cisplatin, which reacts with a first-order reaction with GSH [4]. This interaction between **1** and **2** and glutathione is probably restricted by the existence of sulfur from the thiosemicarbazone ligands coordinated to Pt(II). Thus, although the drawback of cisplatin is the eliminations of its therapeutic activity due to the resistance developed by cancer cells, this might not occur for **1** and **2** since they do not interact with glutathione.

The *in vitro* cytotoxicity studies show that [Pt(EtImt)$_4$]Cl_2 (EtImt = N-Ethyl-13-diazinane-2-thione) exhibits twofold better activity than cisplatin against MCF7, which is comparable with that of **2** (~2-fold stronger than cisplatin) [43]. Organoplatinum(II) complexes, on the other hand, [PtCl(Saf)(8-OQ)], [Pt(Saf-1H)(8-OQ)], [PtCl(Meug)(8-OQ)], [Pt(Meug-1H)(8-OQ)], [Pt(Eteug-1H)(8-OQ)], and [Pt(Eteug-1H)(Q)] (Saf = safrole, Meug = methyleugenol, Meteug = methyl eugenoxyacetate, Eteug = ethyleugenoxyacetate, Q = quinoline, 8-OQ = 8-hydroxyquinolinate, and Q-CO = quinolin-2-carboxylate) were also tested against MCF-7 cells, indicating strong activity (2.09, 1.74, 9.04, 4.86, 1.67, and > 210.18 μM, respectively), which however is comparable with **2** (3.6 μM) [44].

The absence of micronucleus when MRC-5 cells were treated with **1** and **2** confirms *in vitro* non genotoxic behavior. The absence of nuclear abnormalities *in vivo* confirms the non-genotoxic manner of **1** and **2**. Therefore, **2** shows better activity against adenocarcinoma cancer cells, selectivity against cancerous

over normal cells, and better activity than cisplatin, with meaningless or no genotoxicity *in vitro* or *in vivo*. In conclusion, **2** could be a possible candidate for further study as a new chemotherapeutic agent.

4. Experimental

4.1. Materials and instruments

All the chemicals and solvents were spectroscopic and analytical grade and used as received from commercial sources. The FT-IR spectra were recorded on a Shimadzu IRAffinity-1S FT-IR spectrophotometer from 4000 to 400 cm^{-1} using KBr pellets. The ^{1}H and ^{31}P NMR spectra were recorded on a Bruker AC 250 MHz FT-NMR instrument in DMSO-d_6 solution. A UV-1600 PC series spectrophotometer of VWR was used to obtain electronic absorption spectra.

4.2. Synthesis and crystallization of BzimetTSCH, [Pt(BzimetTSCH)Cl]·2H_2O (1) and [Pt(BzimetTSCH)(tpp)]Cl·H_2O·MeCN (2)

BzimetTSCH: BzimetTSCH was synthesized following a previously described method [16]. A mixture of 2-acetylbenzimidazole (5 mmol), thiosemicarbazide (5 mmol), and 1 mL of acetic acid in 50 mL of ethanol was refluxed for 6 h. The product precipitated in a cooled solution, and was filtered and recrystallized from ethanol (max. yield: 80%).

IR (KBr, cm^{-1}): ν(OH) + $\nu(NH_2)$ + ν(NH) 3426(br), 3368(m), 3181(w), 3071(br); ν(C=N) + $\delta(NH_2)$ 1620–1610 (vs); δ(NH) 1543 (s); ν(ring) + δ(NCS) 1499 (s), 1468 (m), 1447 (m); ν(C=S) + γ(CH) 846(m); γ(CH) 766 (m); δ(ring) 656 (s). ^{1}H NMR (ppm) in DMSO-d_6: 12.69 (s, H(^{3}N)), 10.66 (s, H(^{8}N)), 8.53–7.11 (aromatic proton), 2.40 (s, H^{16}C of methyl group)), EtOH used as solvent for the synthesis: 3.44 (q, –CH_2–, EtOH), 1.06 (t, CH_3– EtOH).

4.3. [Pt(BzimetTSCH)Cl]·2H_2O] (1)

A suspension of $PtCl_2$ (0.0665 g, 0.25 mmol) in ethanol (50 mL) and water (10 mL) was stirred half an hour at 40 °C. A solution of the ligand (0.058 g, 0.25 mmol) in ethanol (10 mL) was added to the suspension. The resulting mixture was stirred under reflux for at least 6 h. The mixture was filtered while hot and the filtrate was left for slow evaporation at room temperature. Small red needle crystals were recrystallized from acetonitrile giving X-ray quality red needles.

1: Red crystal; Elemental analysis found: C, 23.50; H, 2.95; N, 13.94; S, 6.83%. Calculated for $C_{10}H_{14}ClN_5O_2PtS$: C, 24.08; H, 2.83; N, 14.04; S, 6.43%. IR (KBr, cm^{-1}): ν(OH) + $\nu(NH_2)$ + ν(NH) 3470(m), 3330(m), 3171(w) 3065(w); ν (C=N) + $\delta(NH_2)$ 1624(vs); δ(NH) 1559(m); ν(ring) + δ(NCS) 1500(s), 1477(vs), 1447(m); ν (C=S) + γ(CH) 842(m); γ(CH) 755(m); δ(ring) 638(m). ^{1}H NMR (ppm) in DMSO-d_6: 8.41 (s, H(^{8}N)), 8.12–7.31 (aromatic protons of BzimetTSCH), 2.25 (s, 3H(^{16}C)).

4.4. [Pt(BzimetTSCH)(tpp)]Cl·H_2O·MeCN (2)

$PtCl_2$ (0.0665 g, 0.25 mmol) in acetonitrile (40 mL) was refluxed for 1 h giving a yellow solution. A mixture of a solution of the ligand (0.058 g, 0.25 mmol) in ethanol (10 mL) and a solution of triphenylphosphine (0.0656 g, 0.25 mmol) in ethanol (10 mL) were added to the yellow solution. The resulting mixture was refluxed for 6 h. The mixture was filtered and the filtrate left for slow evaporation at room temperature, giving X-ray quality reddish-orange prismatic crystals.

2: Reddish-orange crystal; Elemental analysis found: C, 45.55; H, 3.75; N, 10.44; S, 3.92 %. Calculated for $C_{30}H_{30}ClN_6OPtPS$: C, 45.95; H, 3.85; N, 10.72; S, 4.09%. IR (KBr, cm^{-1}): ν(OH) + $\nu(NH_2)$ + ν(NH) 3447(br), 3295(br), 3145(w) 3060(w); ν(C=N) + $\delta(NH_2)$ 1615(s); δ(NH) 1559(m); ν(ring) + δ(NCS) 1500(s), 1477(vs), 1437(s); ν(C=S) + γ(CH) 839(s); γ(CH) 744(s); δ(ring) 632(m); ν(C–P) 515(s), 501(m). ^{1}H NMR (ppm) in DMSO-d_6: 8.16 (s, H(^{8}N)), 7.78–7.07 (aromatic of BzimetTSCH and tpp), 2.55 (s, 3H^{16}C)).

4.5. X-ray structure determination

Suitable crystal was selected for data collection which was performed on a Bruker D8 QUEST diffractometer equipped with graphite-monochromated Mo-Kα radiation. Data reduction was performed with APEX II [45]. Data were corrected for absorption effects using the multi-scan method (SADABS) [46]. The frames were integrated with the Bruker SAINT software package [47] using a narrow-frame algorithm.

The structures were solved with direct methods using SHELXS97 [48] and refined by full-matrix least-squares procedures on F^2 with SHELXL97 [49]. All non-hydrogen atoms were refined anisotropically; hydrogens were located at calculated positions and refined via the "riding model" with isotropic thermal parameters fixed at 1.2 (1.3 for CH_3 groups) times the Ueq of the appropriate carrier atom.

1: $C_{10}H_{10}ClN_5PtS$, $2(H_2O)$, MW = 498.86, monoclinic, space group P21/c, $a = 6.8916(4)$, $b = 21.9580(14)$, $c = 9.6392(6)$ Å, $\alpha = 90$, $\beta = 100.944(2)$, $\gamma = 90°$, $V = 1432.13(15)$ Å^3, $Z = 4$, T = 293 K, ρ (Calcd) = 2.314 g cm^{-3}, μ = 10.138 mm^{-1}, $F(0\ 0\ 0)$ = 944. 33,943 reflections measured, 3273 unique (R_{int} = 0.039). The final R_1 = 0.0249 (for 2984 reflections with $I > 2s(I)$) and $wR(F2)$ = 0.0514 (all data) S = 1.24.

2: $C_{28}H_{25}N_5PPtS$, C_2H_3N, Cl, H_2O, MW = 784.17, monoclinic, space group P21/n, a = 10.505(5), b = 21.722(5), c = 14.104(5) Å, α = 90, β = 95.110(5), γ = 90°, V = 3206(2) Å^3, Z = 4, T = 293 K, ρ (Calcd) = 1.625 g cm^{-3}, μ = 4.609 mm^{-1}, $F(0\ 0\ 0)$ = 1544. 68,047 reflections measured, 5641 unique (R_{int} = 0.072). The final R_1 = 0.0452 (for 4992 reflections with $I > 2s(I)$) and $wR(F2)$ = 0.1116 (all data) S = 1.19.

Crystallographic data (excluding structure factors) for the structures reported in this article have been deposited with the Cambridge Crystallographic Data Center as supplementary publication nos. CCDC-1453335 (**1**) and -1453336 (**2**). Copies of the data can be obtained free of charge on application to CCDC, 12 Union Road, Cambridge CB2 1EZ, U.K. (Fax: (+44) 1223–336-033; E-mail: deposit@ccdc.cam.ac.uk).

4.6. Biological tests

4.6.1. Cells screening

Biological experiments were carried out in DMSO Dulbecco's modified Eagle's medium solutions for **1** and **2**. Stock solutions of **1** and **2** (0.01 M) in DMSO were freshly prepared and diluted with cell culture medium to the desired concentration (0.5–30 μM). Results are expressed in terms of IC_{50} values, which is the concentration of drug required to inhibit cell growth by 50% compared to control, after 48 h incubation of the complexes with cell lines. The cell viability was determined by SRB assay as previously described [22].

4.6.2. Cell cycle

MCF-7 cells were seeded at 10^5 cells/well in six-well plates at 37 °C for 24 h. Cells were treated with **1** and **2** at the indicated IC_{50} values for 48 h. Afterward, the cells were trypsinized and washed twice with phosphate-buffered saline (PBS) and separated by centrifugation. With the addition of 1 mL of cold 70% ethanol, the cells were incubated overnight at –20 °C. For analysis, the cells were centrifuged and transferred into PBS, incubated with RNase (0.2 mg mL^{-1}), and propidium iodide (0.05 mg mL^{-1}) for 40 min at 310 K and then analyzed by flow cytometry using a FACS Calibur flow cytometer (Becton Dickinson, San Jose, CA, U.S.A.). For each sample, 10,000 events were recorded. The resulting DNA histograms were drawn and quantified using FlowJo software (version FlowJo X 10.0.7r2) [50].

4.6.3. Reaction of 1 and 2 with GSH as monitored by UV absorption

This study was performed as reported previously [4].

4.6.4. Micronucleus

A micronucleus test was performed with the following literature procedure [51, 52]. MRC-5 cells were seeded (at a density of 2×10^4 cells/well) in glass cover slips which were afterward placed in six-well plates, with 3 mL of cell culture medium and incubated for 24 h. MRC-5 cells were exposed with **1** and

2 in IC_{50} values for 48 h. After exposure of **1** and **2**, the cover slips were washed three times with PBS and with a hypotonic solution (75 mM KCl) for 10 min at room temperature. The hypotonized cells were fixed by at least three changes of 1/3 acetic acid/methanol. The cover slips were also washed with cold methanol containing 1% acetic acid. The cover slips were stained with acridine orange (5 µg mL^{-1}) for 15 min at 37 °C. After, the cover slips were rinsed three times with PBS to remove any excess acridine orange stain. The number of micronucleated cells per 1000 cells was determined.

4.6.5. In vivo *genotoxicity test*

Small bulbs (1.5–2.0 cm in diameter) of the common onion, *Allium cepa*, were purchased from a local market. Prior to initiating the test, the outer scales of the bulbs and the dry bottom plate were removed without destroying the root primordia. Bulbs of *Allium cepa* were placed in test tubes (10 mL) which were filled with water and placed in the incubator at 25 °C, 50–60% humidity and 12 h/day lighting for 48 h. Aliquots from complex stock solutions (0.01 M in DMSO) were added in the test tubes to incubate the bulbs with the complexes, at 3, 30, and 300 µM. Onion bulbs (two per dose) were exposed to the platinum compounds for 48 h. The roots growing in mineral water were used as a control. The roots were then fixed in 1:3 acetic acid–methanol solutions for 24 h at 4 °C, and finally stored in 70% ethanol. Root tips were hydrolyzed in 6 N HCl at 37 °C for 5 min followed by one wash of 1 min in distilled water before staining in Schiff's reagent for 40 min. After the root caps were removed from well stained root tips, 1 mm of the meristematic was immersed in a drop of 45% acetic acid on a clean slide and squashed into single cells using the eraser end of a pencil to apply pressure. In order to evaluate the rate of the cellular division the microscopic parameter of the mitotic index was determined. All categories were analyzed by counting 1800 cells per concentration (300 cells per slide, total of six slides).

Acknowledgements

CNB and SKH would like to thank (i) the Unit of bioactivity testing of xenobiotics, the University of Ioannina, for providing access to the facilities, (ii) the Atherothrombosis Research Centre of the University of Ioannina for providing access to the flow cytometer, (iii) the Josef and Esther Gani Foundation for the financial support (project number 81455), and (iv) the State Scholarships Foundation of Greece (IKY) for the post doctoral research fellowship of excellence program IKY-Siemens (project number 22957).

Disclosure statement

No potential conflict of interest was reported by the authors.

References

[1] Y. Jung, S.J. Lippard. *Chem. Rev.*, **107**, 1387 (2007).
[2] H. Khan, A. Badshah, G. Murtaz, M. Said, Z.U. Rehman, C. Neuhausen, M. Todorova, I.S. Butler. *Eur. J. Med. Chem.*, **46**, 4071 (2011).
[3] K.J. Barnham, M.I. Djuran, P. del Socorro Murdoch, J.D. Ranford, P. Sadler. *Inorg. Chem.*, **35**, 1065 (1996).
[4] C.N. Banti, L. Kyros, G.D. Geromichalos, N. Kourkoumelis, M. Kubicki, S.K. Hadjikakou. *Eur. J. Med. Chem.*, **77**, 388 (2014).
[5] N.C. Campanella, M. da Silva Demartini, C. Torres, E. Tonon de Almeida, C. Marli Cação Paiva Gouvêa. *Genet. Mol Biol.*, **35**, 159 (2012).
[6] G. Faraglia, D. Fregona, S. Sitran, L. Giovagnini, C. Marzano, F. Baccichetti, U. Casellato, R. Graziani. *J. Inorg. Biochem.*, **83**, 31 (2011).
[7] H. Beraldo, D. Gambino. *Mini-Rev. Med. Chem.*, **4**, 31 (2004).
[8] A.I. Matesanz, I. Leitao, P. Souza. *J. Inorg. Biochem*, **125**, 26 (2013).
[9] A.I. Matesanz, C. Hernández, A. Rodríguez, P. Souza. *Dalton Trans.*, **40**, 5738 (2011).
[10] A. Karaküçük-İyidoğan, D. Taşdemir, E. Elçin Oruç-Emre, J. Balzarini. *Eur. J. Med. Chem.*, **46**, 5616 (2011).
[11] T.T. Tavares, D. Paschoal, E.V.S. Motta, A.G. Carpanez, M.T.P. Lopes, E.S. Fontes, H.F. Dos Santos, H. Silva, R.M. Grazul, A.P.S. Fontes. *J. Coord. Chem.*, **67**, 956 (2014).
[12] A.A. Ali, H. Nimir, C. Aktas, V. Huch, U. Rauch, K.H. Schäfer, M. Veith. *Organometallics*, **31**, 2256 (2012).
[13] M. Poyraz, H. Berber, C. Ogretir. *ARKIVOC*, **8**, 309 (2007).
[14] M. Sari, M. Poyraz, S. Demirayak, O. Büyükgüngör. *Anal. Sci.: X-Ray Struct. Anal. Online*, **21**, x183 (2005).

[15] M. Poyraz, M. Sarı, A. Güney, F. Demirci, S. Demirayak, E. Şahin. *J. Coord. Chem.*, **61**, 3276 (2008).
[16] M. Poyraz, M. Sari, F. Demirci, M. Kosar, S. Demirayak, O. Büyükgüngör. *Polyhedron*, **27**, 2091 (2008).
[17] C.N. Banti, A.D. Giannoulis, N. Kourkoumelis, A. Owczarzak, M. Kubicki, S.K. Hadjikakou. *Dalton Trans.*, **43**, 6848 (2014).
[18] C.N. Banti, L. Kyros, G.D. Geromichalos, N. Kourkoumelis, M. Kubicki, S.K. Hadjikakou. *Eur. J. Med. Chem.*, **77**, 388 (2014).
[19] I. Sainis, C.N. Banti, A.M. Owczarzak, L. Kyros, N. Kourkoumelis, M. Kubicki, S.K. Hadjikakou. *J. Inorg. Biochem.*, **160**, 114 (2016). doi:10.1016/j.jinorgbio.2015.12.013.
[20] D.B. Shpakovsky, C.N. Banti, G. Beaulieu-Houle, N. Kourkoumelis, M. Manoli, M.J. Manos, A.J. Tasiopoulos, S.K. Hadjikakou, E.R. Milaeva, K. Charalabopoulos, T. Bakas, I.S. Butler, N. Hadjiliadis. *Dalton Trans.*, **41**, 14568 (2012).
[21] A. Han, I.I. Ozturk, C.N. Banti, N. Kourkoumelis, M. Manoli, A.J. Tasiopoulos, A.M. Owczarzak, M. Kubicki, S.K. Hadjikakou. *Polyhedron*, **79**, 151 (2014).
[22] O.S. Urgut, I.I. Ozturk, C.N. Banti, N. Kourkoumelis, M. Manoli, A.J. Tasiopoulos, S.K. Hadjikakou. *Mater. Sci. Eng., C*, **58**, 396 (2016).
[23] C.N. Banti, D.C. Charalampou, N. Kourkoumelis, A.M. Owczarzak, M. Kubicki, S.K. Hadjikakou, N. Hadjiliadis. *Polyhedron*, **87**, 251 (2015).
[24] S.J. Berners-Price, R.J. Bowen, P. Galettis, P.C. Healy, M.J. McKeage. *Coord. Chem. Rev.*, **185–186**, 823 (1999).
[25] E. Ramachandran, P. Kalaivani, R. Prabhakaran, N.P. Rath, S. Brinda, P. Poornima, V. Vijaya Padmad, K. Natarajan. *Metallomics*, 4,218 (2012).
[26] M.C. Rodŕiguez-Argüelles, E.C. López-Silva, J. Sanmartín, A. Bacchi, C. Pelizzi, F. Zani. *Inorg. Chim. Acta*, **357**, 2543 (2004).
[27] M.D. Hall, K.A. Telma, K.-E. Chang, T.D. Lee, J.P. Madigan, J.R. Lloyd, I.S. Goldlust, J.D. Hoeschele, M.M. Gottesman. *Cancer Res.*, **74**, 3913 (2014).
[28] A.I. Matesanz, J. Perles, P. Souza. *Dalton Trans.*, **41**, 12538 (2012).
[29] A.A. Ibrahim, H. Khaledi, P. Hassandarvish, H. Mohd Ali, H. Karimian. *Dalton Trans.*, **43**, 3850 (2014).
[30] J.J.P. Stewart. *J. Mol. Model.*, **13**, 1173 (2007).
[31] M. Kajstura, H.D. Halicka, J. Pryjma, Z. Darzynkiewicz. *Cytometry Part A*, **71A**, 125 (2007).
[32] Y.H. Shiao, S.H. Lee, K.S. Kasprzak. *Carcinogenesis*, **19**, 1203 (1998).
[33] K. Zhang, X. Zhao, J. Liu, X. Fang, X. Wang, X. Wang, R. Li. *Oncol. Lett.*, **7**, 881 (2014).
[34] G. Bogdanović, V. Kojić, T. Srdić, D. Jakimov, M.I. Djuran, Ž.D. Bugarčić, M. Baltić, V.V. Baltić. *Met. Based Drugs*, **9**, 33 (2002).
[35] J.C. Dabrowiak, J. Goodisman, A.-K. Souid. *Drug Metab. Dispos.*, **30**, 1378 (2002).
[36] A. Halámiková, P. Heringová, J. Kašpárková, F.P. Intini, G. Natile, A. Nemirovski, D. Gibson, V. Brabec. *J. Inorg. Biochem.*, **102**, 1077 (2008).
[37] O. Torres-Bugarín, M. Guadalupe Zavala-Cerna, A. Nava, A. Flores-García, M. Luisa Ramos-Ibarra. *Dis. Markers*, ID 956835 (2014).
[38] Y. Li, D.H. Chen, J. Yan, Y. Chen, R.A. Mittelstaedt, Y. Zhang, A.S. Biris, R.H. Heflich, T. Chen. *Mutat. Res.*, **745**, 4 (2012).
[39] A. Celik, O. Ogenler, U. Comelekoglu. *Mutagenesis*, **20**, 411 (2005).
[40] S.C. Sahu, S. Roy, J. Zheng, J.J. Yourick, R.L. Sprando. *J. Appl. Toxicol.*, **34**, 1200 (2014).
[41] D.M. Leme, M.A. Marin-Morales. *Mutat. Res.*, **682**, 71 (2009).
[42] A. Lyu, X. Qin, L. Fang, S. Gou. *J. Coord. Chem.*, **69**, 1653 (2016).
[43] A. Zainelabdeen, A. Mustafa, M. Monim-ul-Mehboob, M.Y. Jomaa, M. Altaf, M. Fettouhi, A.A. Isab, M.I.M. Wazeer, H. Stoeckli-Evans, G. Bhatia, V. Dhuna. *J. Coord. Chem.*, **68**, 3511 (2015).
[44] T. Thi Da, L. Thi Hong Hai, L. Van Meervelt, N. Huu Dinh. *J. Coord. Chem.*, **68**, 3525 (2015).
[45] *APEX II*, Bruker AXS Inc., Madison, Wisconsin, USA (2013).
[46] *SADABS*, Bruker AXS Inc., Madison, Wisconsin, USA (2012).
[47] *SAINT*, Bruker AXS Inc., Madison, Wisconsin, USA (2013).
[48] G.M. Sheldrick. *Acta Crystallogr., Sect. A*, **46**, 467 (1990).
[49] G.M. Sheldrick. *SHELXL-97, Program for the Refinement of Crystal Structures*, University of Göttingen, Germany (1997).
[50] S.H. van Rijt, I. Romero-Canelón, Y. Fu, S.D. Shnyder, P.J. Sadler. *Metallomics*, **6**, 1014 (2014).
[51] T. Matsushima, M. Hayashi, A. Matsuoka, M. Ishidate Jr, K.F. Miura, H. Shimizu, Y. Suzuki, K. Morimoto, H. Ogura, K. Mure, K. Koshi, T. Sofuni. *Mutagenesis*, **14**, 569 (1999).
[52] S.K. Sohaebuddin, L. Tang. *Methods Mol. Biol.*, **991**, 25 (2013).